CIVIL ENGINEERING JOURNAL

Article no. 31

THE CIVIL ENGINEERING JOURNAL 3-2023

INVESTIGATION ON THE ROCK-FRAGMENTATION PROCESS OF CONICAL-SHAPED TBM CUTTERHEAD IN EXTREMELY HARD ROCK GROUND

Shijun Chen[1], Xinyu Jin[2], Rucheng Hu[1], Fei Liu[1] and Zhongsheng Hu[1]*

1. *The Electricity Engineering CO., LTD under CREC NO.5 Group, Changsha, Hunan District, 410205, China; 764193226@qq.com, 876111908@qq.com, 2279227407@qq.com, 2575641835@qq.com*
2. *School of Construction Machinery, Chang'an University, Xi'an 710064, China; 2474535362@qq.com*

ABSTRACT

The main objective is to clarify the rock-fragmentation mechanism of a conical-shaped Tunnel Boring Machine (TBM) cutterhead that has rarely been investigated before. The main method is a numerical simulation which is verified by laboratory rock-fragmentation tests. The research process is as follows: Firstly, the numerical model is designed based on cutting mode analysis; Then, the rock sample is synthesized using a Grain-based Discrete Element Method (GDEM) that is verified via scaled rock-fragmentation tests; Finally, a series of numerical simulations are conducted to study the influence of cutterhead cone angle, cutter spacing, and cutter installation angle on the rock-fragmentation performance. The main findings are as follows: First, the rock fragmentation mechanism of conical-shaped TBM cutterhead is free-face-assisted rock breaking; Second, the rock-fragmentation efficiency can be improved by appropriately increasing the conical angle, reducing the cutter spacing, and increasing the cutter installation angle; Third, for the studied granite, the optimal conical angle is 25°, the tilt cutter spacing is suggested to be no more than 70 mm, and the cutter tilt angle is suggested to be no more than 3°. This study reveals the rock fragmentation mechanism of conical-shaped TBM cutterhead and provides suggestions for cutterhead design.

KEYWORDS

Full-face tunnel boring machine, Conical-shaped cutterhead, Disc cutter, PFC, rock-fragmentation mechanism

ABBREVIATIONS

TBM	Tunnel boring machine
GDEM	Grain-based discrete element method
D&B	Drilling and blasting
UCS	Uniaxial compressive strength
BTS	Brazilian Tensile Strength
LCM	Linear cutting machine
CCS	Constant cross-section
PSE	Penetration specific energy
FJM	Flat-jointed method

* Corresponding author

LIST OF SYMBOLS

H	The height of each stage in mm
D	The distance from the cutter penetration point to the stage edge in mm
S	Cutter spacing in mm
α	The cutterhead conical angle
β	The cutter tilted angle
F_{NP}	The peak penetration force;

INTRODUCTION

Full-face Rock Tunnel Boring Machine (TBM) cutterheads can have a cone, dome, or flat shape [1]. The flat-profile cutterhead has been widely used owing to its advantages in geological adaptability, manufacturing, and thrust utilization. Although the other cutterheads are less applied in engineering projects, they have their advantages such as higher structural strength and rigidity [2], higher rock-breaking efficiency [3-4], and lower cutter side slipping level [5]. Zhang et al. [6-7] found that the thrust of a conical-shaped cutterhead can be reduced by properly designing the conical angle. Liu et al. [8] analyzed the adaptability of conical-shaped cutterhead under different ground conditions, and found that the conical-shaped cutterhead is suitable for hard grounds due to its stability during tunneling. Zhang et al. [9] analyzed the vibration characteristics of the conical-shaped cutterhead applied in Dahuofang hydraulic tunnel in China and deduced that the abnormal vibration is caused by the radial alternate rock-breaking load. According to the above review, the study on the structural characteristics and tunneling performance of the conical-shaped cutterhead is very insufficient. Moreover, the relative research mostly stays at the level of theoretical analysis. Furthermore, almost no studies have been conducted and reported for the rock-fragmentation mechanism of conical-shaped cutterhead, resulting in a very limited basis for the cutterhead structure and cutter layout design.

We think that the critical rock-fragmentation mechanism of conical-shaped TBM cutterhead is free-face-assisted rock breaking. This is because the tunnel face is excavated as a multi-step cone by the tilt-installed disc cutters, as shown in Figure 1a. The front steps provide free faces to assist the rock fragmentation of cutters in the back. Thus, the rock fragmentation efficiency may be significantly improved especially in extremely hard rock ground. There are many rock-fragmentation studies based on the free-face-assisted rock-breaking theory, which can provide references for this study. Innaurato et al. [10] conducted indentation tests on hard limestone and extremely hard granite and found that the rock-breaking efficiency can be significantly improved under side-free-face conditions. Ramezanzadeh et al. [11] reported a multi-arm type and a reaming type undercutting roadheader that disc cutters break rock under free-face conditions. Based on these machines, Jiang et al. [12] simulated the rock-breaking process of a disc cutter under side free face and pre-slotting conditions. The results proved that the free-face-assisted methods provide a potential approach for efficiently breaking hard and extremely hard rock. Geng et al. [13-14] proposed the structural scheme of a multi-stage TBM cutterhead and systematically discussed the dynamic evolution mechanism of the side free faces. On this basis, Xia et al. [15] and Zhang et al. [16] carried out full-scale linear cutting tests and simulations on hard granite to study the influence of free-face spacing on the rock-breaking performance. Xu et al. [17] carried out full-scale rotary cutting tests on hard granite to study the critical threshold of free-face spacing. Wang et al. [18] simulated the rock indentation process induced by TBM cutters under different free-face conditions using a grain-based DEM approach, and discovered that there exist two critical thresholds for the free-face height and spacing respectively. Shang et al. [19] simulated the rock fragmentation process caused by TBM disc cutters under free-face-assisted conditions using a peridynamics model. The results can guide the cutter layout design. Bilgin et al. [20] thought that waterjet-assisted cutting may be the most promising method when used in combination with mechanical cutting tools. The essence of a high-pressure hydraulic coupling rock breaking is to use high-pressure abrasive water jet to prepare kerfs in the surrounding rock to form free faces, to improve the rock-breaking efficiency of cutters. Based on this, Zhang et al. [21] carried

out full-scale linear cutting tests induced by a disc cutter on hard rock that narrow kerfs had been prepared by waterjet. Results show that the cutter's normal force was decreased by 40% and the rock-breaking efficiency was significantly improved. Geng et al. [22] built rock indentation numerical models of disc cutters under different kerf conditions using a Grain-based Discrete Element Method (GDEM). The influence of the precut-kerf structure on the rock-fragmentation mechanism was investigated and some suggestions for high-efficiency rock breaking were given. Cheng et al. [23] carried out an experimental and numerical study on the indentation behavior of TBM disc cutter on hard-rock precutting kerfs by high-pressure abrasive waterjet. The results show that the average peak force decreases significantly with the increase of the kerf depth. Li et al. [24-25] conducted full-face linear cutting tests and numerical simulations on pre-grooved rock to study the influence of cutting modes, pre-groove depth, and pre-groove spacing on assisted rock breaking performance. The results can inspire the design of waterjet-coupling TBMs. Zhou et al. [26] conducted static penetration tests on a rock with pre-cutting grooves to study the influence of groove depth on the rock-breaking mechanism.

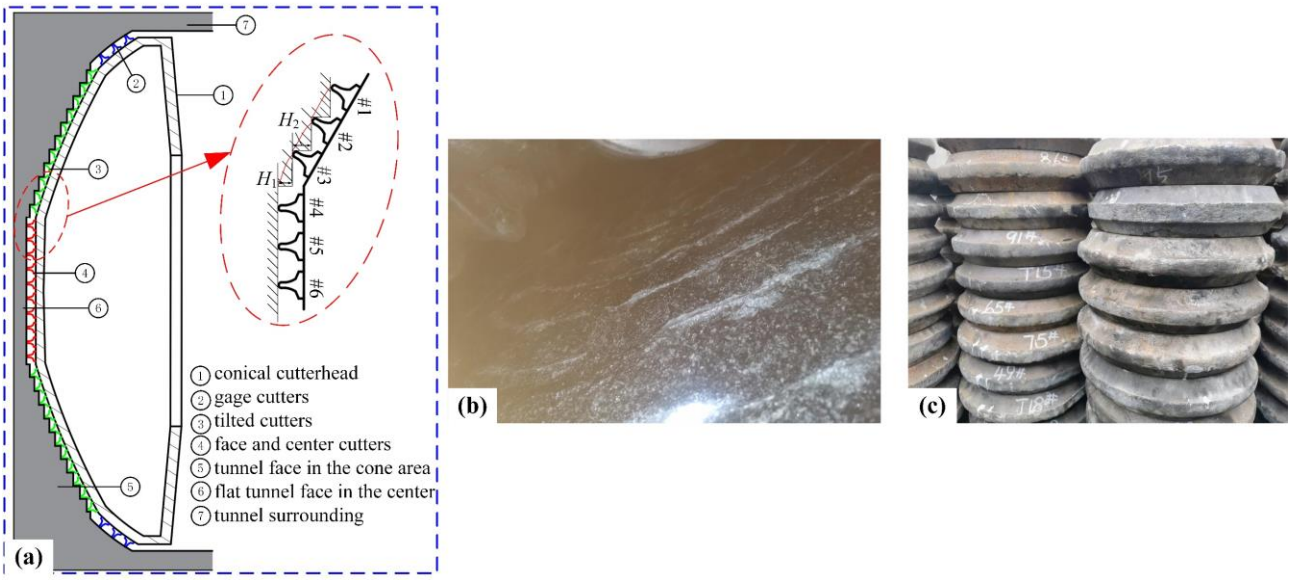

Fig. – 1 (a)Schematic diagram of rock excavation by a conical TBM cutterhead; (b) tunnel face in the extremely hard rock; (c) severe cutter wear.

The above study shows that the free face is an effective method to improve the rock-breaking efficiency of disc cutters. Exploration and research have been carried out based on various TBM equipment and cutterhead. However, there are few reports on the mechanism of free-face-assisted rock breaking of conical-shaped cutterhead, although it is much easier for practical implementation than the other designs such as the undercutting TBM, multi-stage cutterhead, and waterjet-assisted TBM. As a result, aiming at the problem encountered in the Zijing tunnel that the rock-breaking efficiency is low and cutter consumption is high, a conical-shaped cutterhead is assumed to be applied in the extremely hard rock ground and the rock-fragmentation mechanism is investigated. Firstly, a GDEM numerical model for the rock-fragmentation process of a conical-shaped cutterhead was built. Then, factors of cutterhead cone angle, cutter spacing, and cutter installation angle were studied in detail to explore their influence on the rock-fragmentation performance. This study can fill in gaps in the rock-fragmentation mechanism of the conical-shaped TBM cutterhead and can provide some suggestions for the cutterhead design.

PROJECT OVERVIEW

As shown in Figure 2, the Zijing Tunnel is between Yingxiu Town and Gengda Town in Sichuan Province, China. The tunnel has an entrance mileage of DK35+667 and an exit mileage of DK46+084, with a total length of 10413 m. The drilling and blasting (D&B) method is applied for 414 m excavation, a TBM is applied for 5199 m excavation, and the drilling and splitting (D&S) method is applied for 4800 m excavation. It is a single tunnel with double tracks and a maximum buried depth of about 709m. An open-type TBM was developed for the 5199 m-length tunnel excavation. The total length of the TBM is 222 m, the length of the main machine is 25 m, the total weight of the TBM is about 2500 t, the total installed power is 7613.2 kW, and the maximum thrust is 27586 kN. The cutterhead is a flat-face type and is 10.23 m in diameter. A total of 4 double-ring center cutters (432 mm in diameter) and 58 single-ring face and gage cutters (483 mm in diameter) are installed on the cutterhead. As shown in Fig. 1(b), when the TBM excavates in the mileage from DK 37+000 to DK 37+419, extremely hard diorite with uniaxial compressive strength (UCS) of approximately 250 MPa and Brazilian Tensile Strength (BTS) of approximately 20 MPa was frequently encountered; when the TBM excavates in the mileage from DK 37+509 to DK 39+150, hard granite whose UCS was approximately 180 MPa was frequently encountered. When the TBM excavates in these grounds, the rock is mainly ground into powder or small chips, resulting in a very low advancing rate and severe cutter wear, as shown in Fig. 1(c). For example, the advance distance per day and the TBM thrust is given in Fig. 3 when the TBM excavates in the mileage from DK 37+000 to DK 37+400 in hard diorite-dominated ground. The TBM was stopped due to the maintenance of the main belt from December 28, 2022, to February 17, 2023. Thus, there are no data for this period. The average thrust is approximately 24870 kN, which is 90% of the maximum thrust. However, the average advance distance per day is 8.2 m per day, which is quite low. There are some days that the advance distance is lower than 4 m, indicating that the advance rate and rock-breaking efficiency are very low.

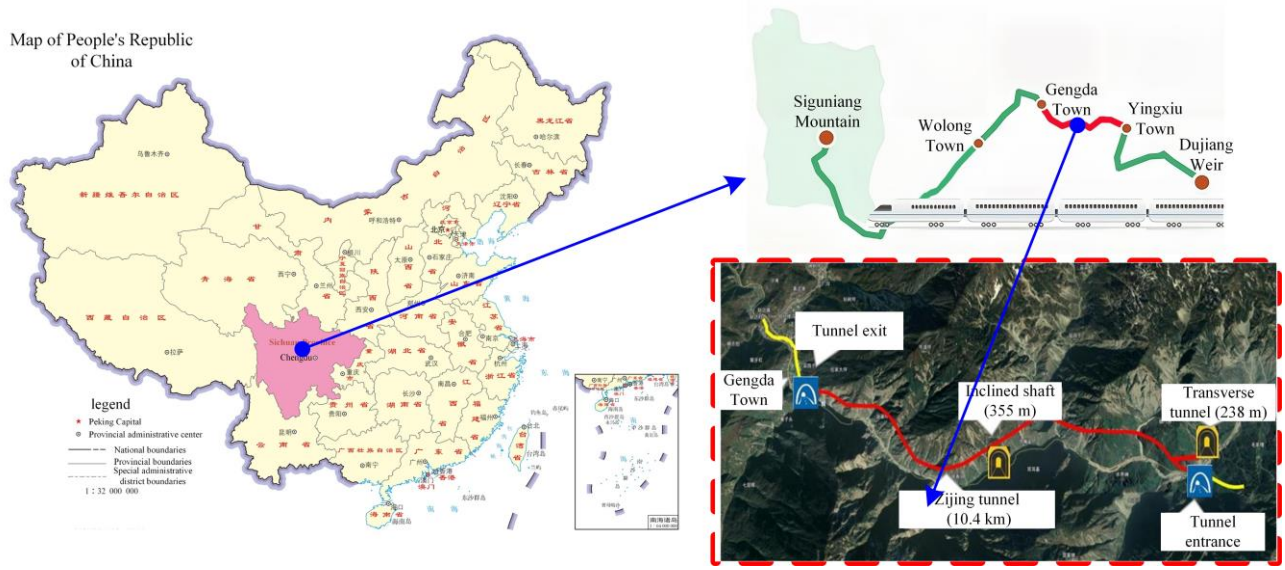

Fig. 2 - General view of the location of the studied Zijing Tunnel Project

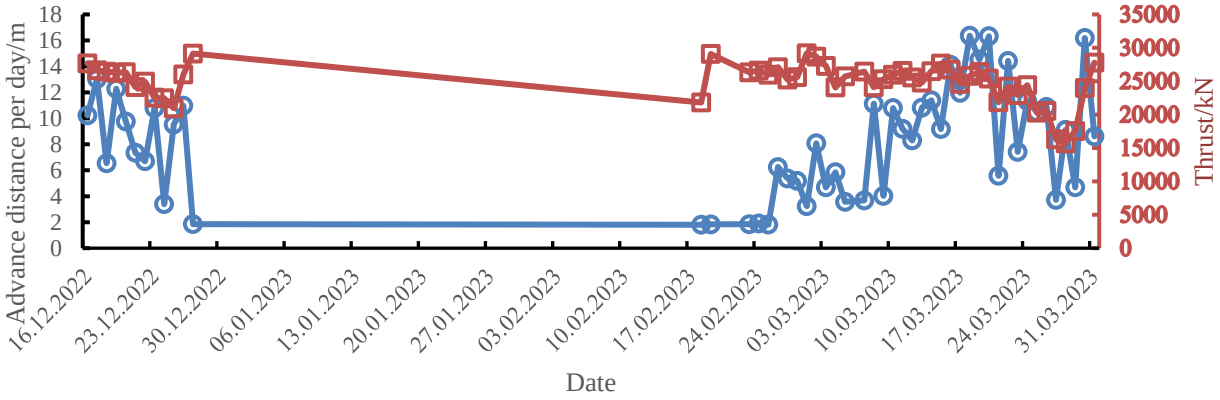

Fig. 3 - The advance distance per day and the TBM thrust in the mileage from DK 37+000 to DK 37+400

CALCULATION INSTRUCTIONS OF THE NUMERICAL SIMULATION

Calculation model

PFC2D software is used in this paper. According to the schematic diagram of rock excavation by a conical TBM cutterhead shown in Fig. 1(a), the typical calculation model is built as illustrated in Figure 4. Three normal cutters numbered #4 to #6 and three tilted cutters numbered #1 to #3 are considered. As several studies (e.g. [10, 27, 28]) have verified the appropriateness of the two-dimensional equivalent model, disc cutter indentation is considered a plane problem. Six cutters are included in the numerical model considering the simulation cost. The rock-breaking of the six cutters can represent the general performances of the normal and tilted cutters.

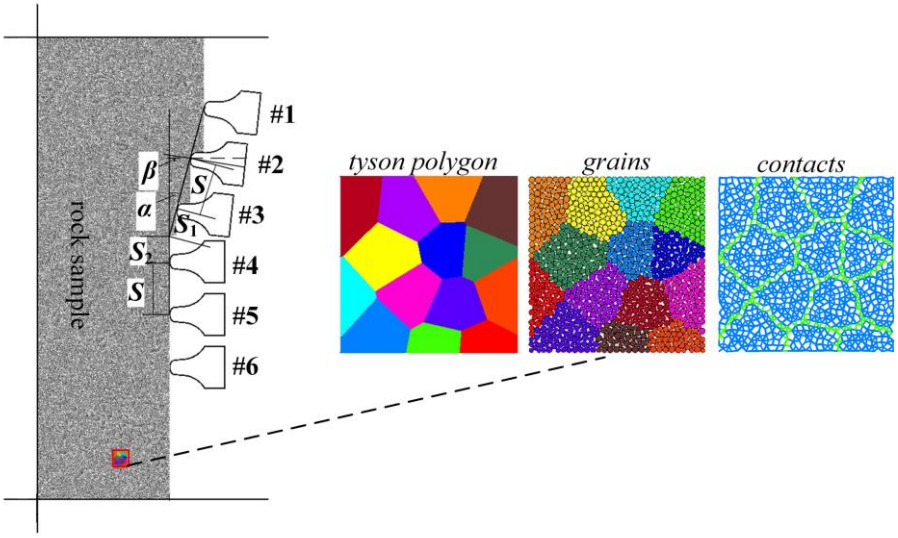

Fig. 4 - Numerical calculation model

Because the essence of the rock-fragmentation of conical-shaped cutterhead is free-face-assisted rock breaking, the height (H) of each stage and the distance (D) from the cutter penetration point to the stage edge are the critical structural factors affecting the rock fragmentation performance. Thus, three factors that determine the H and D are considered in the calculation model, which is the cutter spacing (S), the cutterhead conical angle (α), and the cutter tilted angle (β). It is assumed that the spacing of the normal cutters and the spacing of the tilted cutters are equal, both are S, and the spacings in the transition area are $S_1 = S_2 = S/2$. The cutterhead conical angle (α)

represents the angle between the enveloped surface of the ring tips of the tilted cutters and the flat surface in the front. The cutter tilted angle (β) represents the angle between the center surface of the cutter ring and the vertical line of the cone surface. The disc cutters are modeled by rigid wall elements in the PFC2D software. The maximum penetration displacement of the cutters is 3 mm. Referring to existing research [22], the penetration speed is set as 0.02 m/s, and the time step is 5.5×10^{-8} s to ensure the quasi-static penetration state.

Rock can be regarded as a granular discrete medium. Thus, the rock sample was synthesized using a GDEM approach. This approach is an optimization of the regular Parallel-Bonding (PB) method to solve its shortage of large errors for the UCS/BTS ratio [29]. The interlocking friction along irregular rock grain boundaries can be simulated by using the GDEM approach, and the fractures that follow the grain boundaries and traverse the grain body can be both simulated. This approach is becoming popular and has been applied by several researchers, proving its reasonability and effectiveness [17, 28, 30-31]. The GDEM modeling process is shown in Fig. 4. Firstly, the Tyson polygon algorithm is used to divide the rock into different polygons. Secondly, the rock area is filled with spherical particles, and the particles are grouped according to the polygons to characterize different rock grains. The color of rock grains in the same group is the same. Thirdly, the contact bonds with different meso mechanical parameters are added between the particles and the walls. The contacts between the particles are divided into intragranular contact (blue short line) and intergranular contact (green short line). The intragranular contact and intergranular contact parameters are calibrated and assigned. The contacts between the particles and the walls are not illustrated.

Proper selection of the particle packing and contact parameters are a critical problem that determines the accuracy of the DEM model. However, for a particle aggregating system, the relationships between the particles' mesoscopic parameters and the sample's macroscopic physical properties are very complex and cannot correspond one-to-one. As a result, scholars usually use a trial-and-error method to obtain the mesoscopic parameters of particles based on UCS and BTS tests and simulations, which is also called parameter calibration. UCS and BTS tests were carried out to obtain the macroscopic physical parameters of rock samples. UCS tests are performed on trimmed core samples, which have a diameter of 50 mm and a length-to-diameter ratio of 2. BTS tests are conducted on core samples having diameter of 50 mm and a length-to-diameter ratio of 1. Groups of UCS and BTS tests were simulated for the rock synthesized using the GDEM approach described in the preceding paragraph. To reduce the number of independent parameters during calibration, several assumptions were made according to previous publications [28-29, 32-33]: (i) the density of the particles was determined by the realistic density of the rock material, (ii) the particle radius was smaller than 0.9 mm and the porosity was approximately 0.1 for two-dimensional models, (iii) Young's modulus was determined by the effective modulus 'emod' and the Poisson's ratio was determined by the stiffness ratio 'kratio' and 'pb_kratio', (iv) the 'emod' of the particles and bonds was set the same and so was the stiffness ratio. During the UCS and BTS simulations, the loading speed was set to 0.02 m/s with a time step of 5.5×10^{-8} s to ensure that the simulation is quasi-static penetration. The obtained meso mechanical parameters of granite are shown in Table 1, and the obtained macro mechanical parameters of rock are shown in Table 2. The micromechanical parameters of Set 1 are used for model calculation, and the micromechanical parameters of Set 2 are used for model verification. The errors between the elastic modulus, Poisson's ratio, UCS, and BTS of the rock model and the actual rock are within 5%, which indicates that the numerical model is reliable. To further prove the GDEM accuracy and discuss the sensitivities of particle parameters on the results, another UCS and BTS simulations were conducted using the PB method. The obtained parameters and properties are listed in Set 1-1. Compared with Set 1, the only difference in the mesoscopic parameter setting is ignoring the grain representation. Results listed in Tab. 2 show that the E and υ of Set 1 and Set 1-1 are almost the same since they are determined by the 'emod', 'kratio' and 'pb_kratio' as assumed before. The UCS and BTS of Set 1-1 are obviously increased and decreased respectively compared with those of Set 1, confirming the effectiveness of GDEM in improving the model accuracy. Comparing Set 2 with Set 1, the particle packing

parameters including the ball radius, porosity, and grain size are different. Thus, the contact parameters are also varied to obtain the target values of E, υ, UCS, and BTS. The above analyses indicate that the simulation results are sensitive to the particle packing and contact parameters. That's why great efforts have been spared by scholars to develop modeling and calibration approaches. Following the above assumptions during calibration, a unique set of contacting parameters can be obtained for a set of given packing parameters. This can ensure the stability of the simulation results.

Tab. 1 - The mesoscopic parameters of the rock sample (note: Set 1 and Set 2 use GDEM and Set 1-1 uses PB method)

Parameters	Set 1	Set 1-1	Set 2
Ball density (kg/m3)	2610	2610	2610
Porosity	0.1	0.1	0.075
Ball radius (mm)	0.5±0.1	0.5±0.1	0.025±0.05
emod /GPa	20	20	19
kratio	1.2	1.2	1.4
Intragranular friction coefficient	0.52	0.52	0.52
Intergranular friction coefficient	0.44		0.44
pb_emod (GPa)	20	20	19
pb_kratio	1.2	1.2	1.2
Intragranular pb_ten (MPa)	90±9	90±9	200±20
Intergranular pb_ten (MPa)	70±7		50±5
Intragranular pb_coh (MPa)	90±9	90±9	200±20
Intergranular pb_coh (MPa)	90±9		50±5
Average grain size /mm2	3.2	/	1.6

Tab. 2 - The mechanical properties of the actual rock and the rock sample (note: Set 1 and Set 2 use

Properties	Test	Set 1		Set 1-1		Set 2	
		Sample	Error/%	Sample	Error/%	Sample	Error/%
Modulus, E/GPa	38.6	40.1	3.9	40.1	3.9	39.6	2.5
Poisson's ratio,υ	0.170	0.1697	0.2	0.1642	0.3	0.168	1.1
UCS/MPa	177.9	176.8	0.6	191.6	7.7	185.3	3.9
BTS/MPa	12.6	12.0	2.4	11.8	6.3	12.64	0.3

GDEM and Set 1-1 uses PB method)

Introduction to the test platform

As shown in Figure 5, a small-scale linear cutting machine (LCM) was used in this study to verify the numerical model. The rationality of using small-scale LCM to investigate the rock-breaking mechanism of disc cutters should be stated first. According to several similar studies [34-36], the rock-breaking theory of small disc cutters is almost identical to that of full-scale disc cutters, considering the critical problems of dense core and side crack evolution. In addition, the stiffness of the small-scale LCM can be ensured by using a thick steel frame, high-strength bearing, and strong cutter ring. As a result, small-scale tests are becoming more and more popular in investigating the rock-breaking process of TBM disc cutters. The applied small-scale LCM can perform linear rock-breaking tests under different confining pressure conditions. The working principle of this platform is similar to that of a full-scale LCM [15, 25, 37-39]. It has the advantages of a similar rock-breaking mechanism to the actual TBM cutter, a high utilization rate of rock samples, convenient confining pressure loading, and convenient rock-breaking load acquisition. A disc cutter and a three-directional force sensor are installed on the vertical lifting plate. The cutter is adjusted to the set cutting position via a screw and is then fixed. The rock is placed into the inner layer of the double-layer specimen box. The confining pressure sensor and lateral hydraulic cylinder are installed between the inner and outer layers of the specimen box for rock clamping and confining pressure loading (maximum to 40 MPa). The specimen box is integrally installed on two horizontal slide rails and moves along the horizontal direction through the drive system composed of a stepping motor, reducer, and lead screw. Based on this, the relative linear rolling cutting motion between the cutter and the rock can be realized, which is consistent with a full-scale LCM. The test platform can accommodate the largest cuboid rock sample of 500 × 200 × 100 mm. Using the three-directional force sensor, the cutter's normal force, rolling force, and side force can be collected and recorded. The data sampling frequency is 5 Hz and the sampling accuracy is 1 N. For rock-breaking by full-scale disc cutters, the linear cutting speed is approximately 1.5 m/s and the data sampling frequency is higher than 20 Hz [40]. It means that the rock-breaking forces are sampled at the maximum cutting distance interval of 75 mm. For the small-scale tests, although the data sampling frequency is only 5 Hz, the linear cutting speed can be very low (1.2 mm/s in this study), resulting in a sampling interval of 0.24 mm, which can ensure the integrity of the sampled data. The normal force in the small-scale test is usually several kilonewtons, meaning that the relative sampling accuracy is higher than 0.1%.

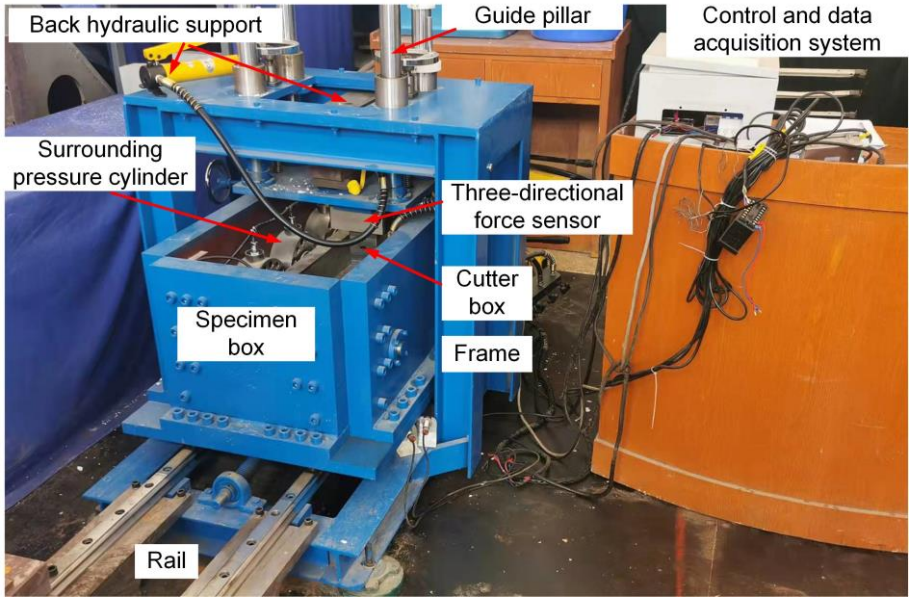

Fig. 5 - Small-scale linear cutting machine (LCM)

Verification of the numerical model

The numerical model is tested and verified to prove the reliability of the numerical model. As discussed above, the essence of the rock fragmentation of conical cutterhead is free-face-assisted rock breaking. As a result, a small-scale linear cutting test under a side-free-face condition and a small-scale cutter penetration simulation under a side-free-face condition were performed and compared.

The rock-breaking test result is shown in Figure 6(a). The rock sample in the test is 320×100×100 mm. The sample surface was first trimmed and polished, and then placed into the specimen box and fixed. Two steel blocks with a thickness of 30 mm were placed on the bottom side of the rock so that a side-free face with a height of 40 mm was prepared. The spacing between the cutting line and the side-free face was 15 mm. The applied cutter was a small-scale constant cross-section (CCS) cutter with a diameter of 43.2 mm and a ring tip width of 1.2 mm. During the test, the cutter remained stationary, and the specimen box was moved linearly along the rails at a speed of 1.2 mm/s driven by the stepping motor. The peak normal force of the test was recorded as 6.7 kN, and several triangular rock debris was formed on the right free face.

The rock-breaking simulation result is shown in Figure 6(b). The rock sample is 100×60 mm and the height of the side free face is 40 mm. The spacing between the cutter penetration point and the side free face is 15 mm. The sizes of the cutter are identical to those of the cutter applied in the test. The rock sample was synthesized using the Set 2 microscopic parameters given in Table 1 and the mechanical properties of the rock sample are shown in Table 2. The cutter penetrated the rock with a speed of 0.02 m/s until the rock in the free-face side was split into a triangular chip. Using the equation proposed by Xu et al. [17], the two-dimensional penetration force obtained from the simulation was converted into an equivalent value of a three-dimensional situation as 7.3 kN, with an error of 11% compared with the test. The shape of the rock debris was like a triangle, which was very similar to the test result. Parameters in Set 2 rather than Set 1 were used to build the scaled indentation model considering the coordination of particle size and cutter tip width. The similarity of the rock-breaking results for the scaled test and simulation can verify the reliability of the GDEM numerical model. Thus, full-scale simulations considering large particles of Set 1 are justified.

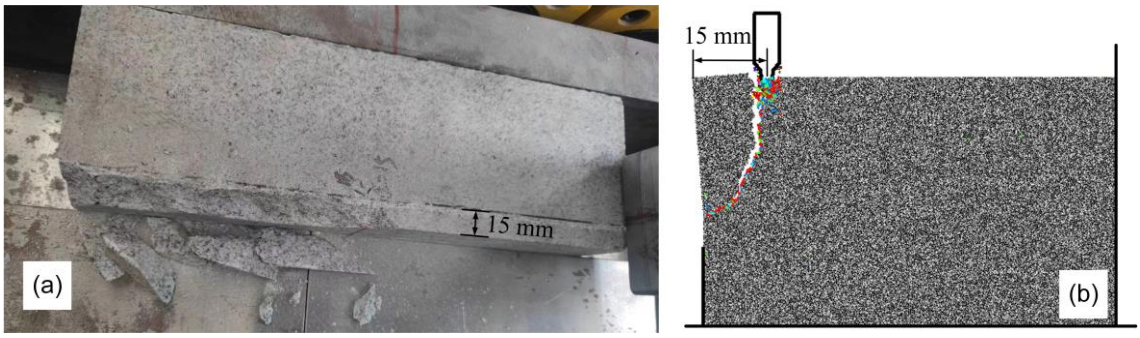

Fig. 6 - Comparison of the rock-breaking test and simulation

SIMULATION RESULTS AND DISCUSSION

Influence of cutterhead conical angle on rock breaking

To explore the influence of cutterhead conical angle α on rock breaking, 10 groups of simulations were performed. The independent variable α was set as 5°, 8°, 10°, 13°, 15°, 18°, 20°, 23°, 25° and 28°, respectively. The dependent variables were the penetration force of each cutter and the rock debris area. The constant variables through the simulations were cutter spacing (S, 80 mm) and cutter tilted angle (β, 0°).

The rock-breaking performance under different α is shown in Figure 7. With the increase of α, the rock-crushing performance induced by face cutters #4 to #6 does not change obviously. The

main damage pattern is shear-type crushing beneath the cutter tip. Some radial cracks initiate and propagate along the penetration direction, while few lateral cracks develop. This results in only a little small rock debris between neighbouring cutters but much powder beneath the cutters. This is possible because the *S* of 80 mm is too large for the studied hard rock to achieve high-efficiency rock-breaking by the normal cutters.

With the increase of *α*, the rock-crushing performance induced by tilt cutters #1 to #3 changed significantly. When *α* is smaller than 15°, even if some macro cracks are generated beneath the tilt cutters, there is little large rock debris. When *α* is greater than 18°, the macro cracks beneath the tilt cutters extend toward the side free faces, generating triangular rock debris. When *α* is greater than 25°, large rock debris forms between the three tilt cutters. This is because the height of the free face ($H=S\cdot\sin\alpha$) increases and the distance ($D=S\cdot\cos\alpha$) between the penetration point and the side free face decreases, both improving the promoting effect of side free face on crack propagation and thus improving the rock-breaking efficiency of the tilt cutters. This is because the rock-breaking difficulty is in positive and negative correlation with *D* and *H*, respectively, according to Geng et al. [14]. The rock-breaking of conical-shaped cutterhead also follows this law.

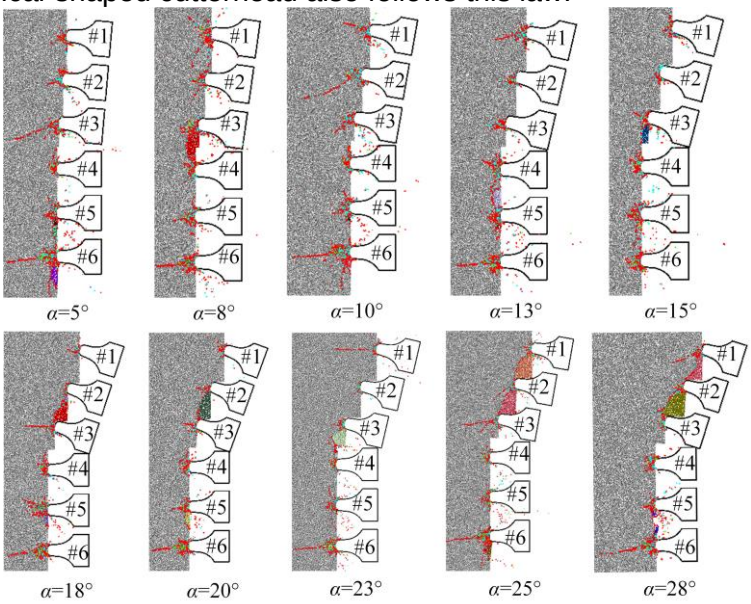

Fig. 7 - Rock-breaking performance under different cutterhead conical angles, α

As shown in Figure 8, the average values of the peak penetration force (F_{NP}) of the tilt cutters #1 to #3 are lower than those of the normal cutters #4 to #6. This is because the side-free face can effectively reduce the cutter penetration force which has been proved by some previous studies [10, 13, 14]. Furthermore, the average F_{NP} of normal cutters does not change with the increase of *α*, while the average F_{NP} of tilt cutters is obviously affected by *α*. These results indicate that conical angle *α* can help reduce the cutter penetration force and hence improve the rock-breaking efficiency. When *α* increases from 10° to 15°, there is a significant drop in F_{NP}; after that, the F_{NP} is generally stable as *α* increases. This means that for the studied models there exists a critical angle of 15° that the promoting effect for reducing the cutter penetration force by the free faces induced by the conical angel *α* is fully exploited. The peak penetration force of the tilt cutters is estimated to be reduced by approximately 50% compared with that of the normal cutters when *α* is larger than 15°.

The overall penetration specific energy (PSE) of the six cutters #1 to #6 is calculated as the energy required to produce unit volume (area for two-dimensional situation) of rock debris, which is used to evaluate the rock-breaking efficiency. For three-dimensional conditions, the rock-breaking specific energy is mainly affected by cutter rolling force and rock chip area [38]. However, in two-dimensional conditions, the cutter rolling force is ignored and thus the cutter penetration force is used to calculate PSE. This indicator is reasonable and has been widely applied in two-dimensional simulations and tests [17, 22]. As shown in Figure 8, as *α* increases from 5° to 10°, the *PSE* increases

to a peak value; as *α* increases from 10° to 25°, the *PSE* decreases to the lowest value. This is because the *PSE* is determined by both the penetration force and the rock debris area. Even though the F_{NP} will not decrease significantly after the *α* is larger than 15°, more debris will be produced after the *α* is larger than 25°. Based on the above analysis, it is suggested that the critical value of the cutterhead conical angle *α* is 25°, to achieve low cutter penetration force and high rock-breaking efficiency.

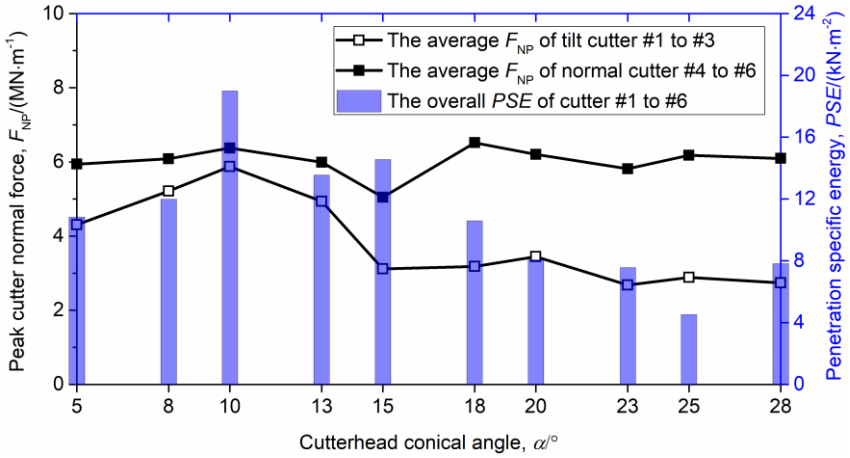

Fig. 8 - Rock-breaking normal force and specific energy under different cutterhead conical angles, α

Influence of cutter spacing on rock breaking

To explore the influence of cutter spacing *S* on rock breaking, 8 groups of simulations were performed. The independent variable *S* was set as 60, 65, 70, 75, 80, 85, 90, and 95, respectively. This parameter setting is based on the common rule that the TBM cutter spacing for hard rock conditions is usually in the range of 60-90 mm [24-25]. The dependent variables were the penetration force of each cutter and the rock debris area. The constant variables through the simulations were cutterhead conical angle cutter spacing (*α*, 15°) and cutter tilt angle (*β*, 0°).

The rock-breaking performance at different *S* is shown in Figure 9. The macro cracks beneath the face cutters #4 to #6 are difficult to connect, and thus there is no large rock debris produced between the neighbouring face cutter. This is because the rock is too hard and the confining stress that may promote rock breaking is not considered in this study [39]. When *S* is smaller than 70 mm, the macro cracks beneath the tilt cutters #1 to #3 can connect, and thus large triangular rock debris can be produced. When *S* is larger than 70 mm, it is difficult to produce large rock debris between neighbouring tilt cutters. The reasons are as follows: firstly, it has been proved that the increase of the free-face height (H=S·sin*α*) and the decrease of the distance (D=S·cos*α*) between the penetration point and the side free face can promote the rock-breaking performance, and vice versa [15]; Secondly, although *H* increases with the increase of *S* and the auxiliary rock-breaking of the free face can be promoted, *D* also increases with the increase of *S* and the promotion effect of free face on rock breaking is weakened and further suppresses the positive effect of *H*. Therefore, the rock-breaking performance of the tilt cutter in the conical area decreases with the increase of the cutter spacing.

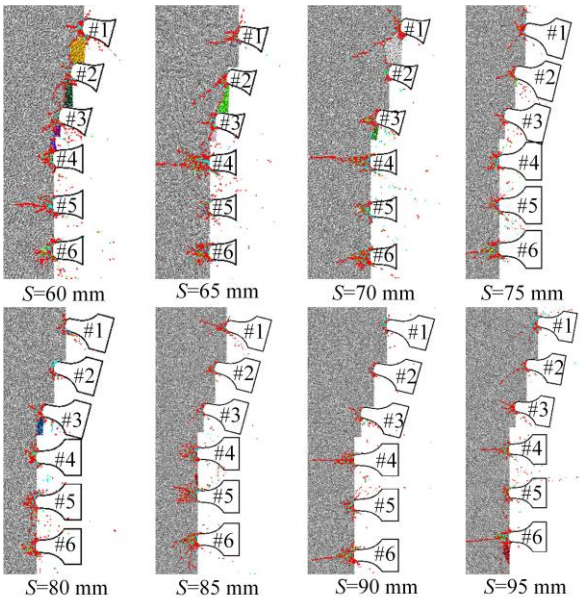

Fig. 9 - Rock-breaking performance under different cutter spacing, S

As shown in Fig. 10, the average values of the peak penetration force (F_{NP}) of the tilt cutters #1 to #3 are lower than those of the normal cutters #4 to #6. Furthermore, the average F_{NP} of normal and tilt cutters does not change obviously with the increase *S*. This is because the rock is too hard and it is difficult for the cracks initiating from neighbouring cutters to propagate and intersect with each other. There exists a critical value of 70 mm for *S* considering the *PSE*. When *S* is lower than 70 mm, the *PSE* is lower than those of the models when *S* is larger than 80 mm. This is because when *S* is lower than 70 mm, large rock debris can be formed between neighbouring tilt cutters. It is acknowledged that too small cutter spacing will increase the number of cutters and increase the difficulty of cutter installation. Thus, based on the studied models, it is suggested that the optimal cutter spacing for the tilt cutters is smaller than 70 mm, and the cutter spacing for the normal cutters should be smaller than that of tilt cutters.

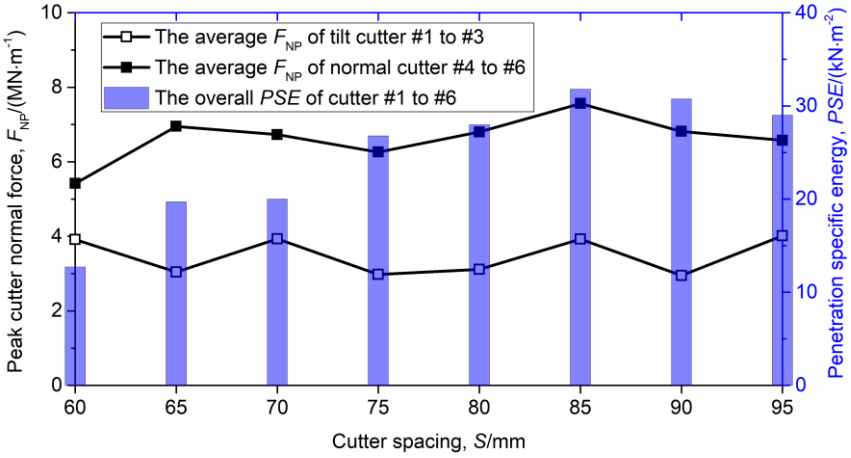

Fig. 10 - Rock-breaking normal force and specific energy under different cutter spacing, S

Influence of cutter tilt angle on rock breaking

To explore the influence of cutter tilt angle *β* on rock breaking, 9 groups of simulations were performed. The independent variable *β* was set as 0°, 1°, 3°, 5°, 7°, 9°, 11°, 13° and 15°, respectively. The dependent variables were the penetration force of each cutter and the rock debris area. The

constant variables through the simulations were cutterhead conical angle cutter spacing (α, 15°) and cutter spacing (S, 80 mm).

The rock-breaking performance at different β is shown in Figure 11. The rock-breaking performance in the rock area of the normal cutter has no obvious change trend. The crack beneath the # 6 normal cutter is the deepest, because it is located at the bottom, and it is less affected by the rock breaking of neighbouring cutters. When β is larger than 9°, there is only small rock debris generated beside the #3 tilt cutter in the conical area. When β is lower than 7°, side cracks initiate from the bottom of the tilt cutters and begin to extend to the side-free face, and thus large rock debris begins to be produced beneath the tilt cutters. The weight of rock debris decreases with the increase of β.

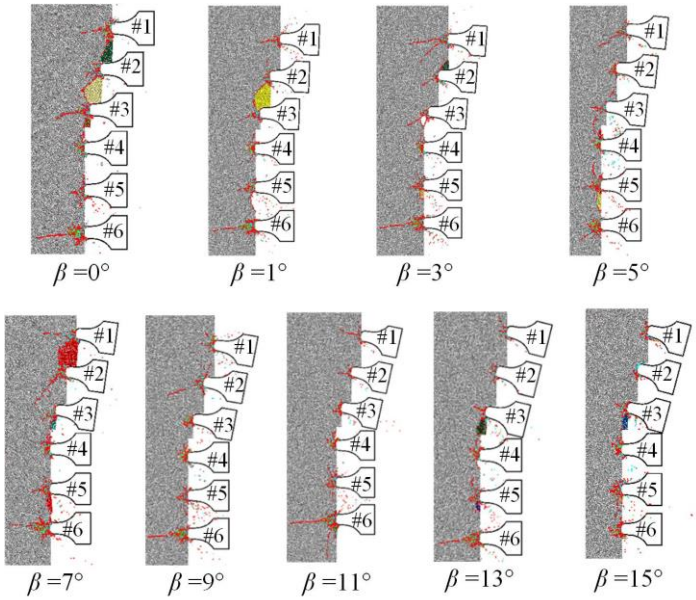

Fig. 11 - Rock-breaking performance under different cutter tilt angles, β

As shown in Figure 12, the average values of the peak penetration force (F_{NP}) of the tilt cutters #1 to #3 are lower than those of the normal cutters #4 to #6. The F_{NP} of the normal cutters #4 to #6 does not change with β because the arrangement of the normal cutters is not affected by β. When β is lower than 5°, the F_{NP} of the tilt cutters increases with the increase of the β. When β is between 7° to 13°, the F_{NP} of the tilt cutters decreases with the increase of the β. It means that there exists a critical value of 5° for β at which the rock-breaking performance is the worst, and this is in accordance with the results shown in Figure 10. If the model that β equals 7° is not considered, the *PSE* increases to the peak value when β is 9° and then decreases. The *PSE* of the model that β equals 7° is abruptly low because the rock-breaking process is somehow randomized and a large rock debris is produced between tilt cutter #1 and #2. The *PSE* of the models that β is larger than 13° is relatively low because the cutter is tilted and the ring tip penetrates the rock like a wedge, resulting in low penetration force. Even so, it is suggested that β should be close to 0° or no more than 3° considering both the rock-breaking performance and the penetration force.

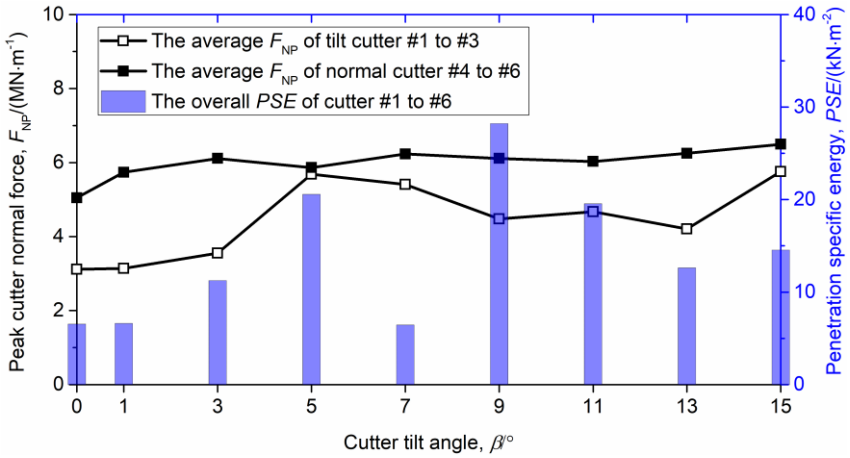

Fig.12 - Rock-breaking normal force and specific energy under different cutter tilt angles, β

Discussions considering previous studies

We reviewed previous studies on the rock-breaking mechanism of conical-shaped cutterhead but found no valuable information. However, many rock-breaking studies under different side-free-face conditions can provide inspiration. Some representative studies are shown in Figure 13. The UCS of the studied rocks varies from 64 MPa to 234 MPa, covering medium strength, hard, and extremely hard rock. The laboratory test methods include static penetration based on simplified indenters and rotary or linear cutting based on full-scale disc cutters. As discussed before, the working principle of the applied small-scale LCM in this study is identical to that of a full-scale LCM. The numerical simulation methods in previous studies include finite element method (FEM) (Figure 13e), GDEM (Figure 13f), PB (Figure 13g), and flat-jointed method (FJM) (Figure 13h). The successful application of these methods confirms the rationality of the numerical simulation in this study.

According to previous studies, the typical rock-fragmentation mode under side-free-face conditions is 'oblique splitting'. The phenomenon is that a macro crack initiates from the cutter penetration point and then propagates to the bottom of the side free face, generating a triangular cross-section chip. This phenomenon is also observed in this study for rock fragmentation by conical-shaped cutterhead. As shown in Figure 7, 9, and 11, the rock beneath several tilt cutters is broken in the 'oblique splitting' mode, exploiting the side-free face to improve the rock-breaking performance. The critical parameters considered in previous studies are *D* and *H*. Previous studies find that there is usually a critical threshold for the ratio of (*D*/*H*). When *D*/*H* is smaller than the critical threshold, the side-free face can help improve the rock-breaking efficiency. The critical thresholds of *D*/*H* for the studies by Innaurato et al.[10], Xu et al.[17], Xia et al.[15], Geng et al.[14], and Jiang et al.[12] are 2.5, 1.0, 0.5, 1.2, and 0.5, respectively. This value is affected by the rock type and cutter geometry. In this study, the influences of *α*, *S*, and *β* on cutter penetration force and specific energy are analyzed considering their relationship with *D* and *H*. It is deduced that *D*/*H* denotes *ctg*(*α*) and the critical threshold is approximately 2.1 when *α* is 25°. Besides, the parameter *S* and *β* also affects the rock-breaking performance.

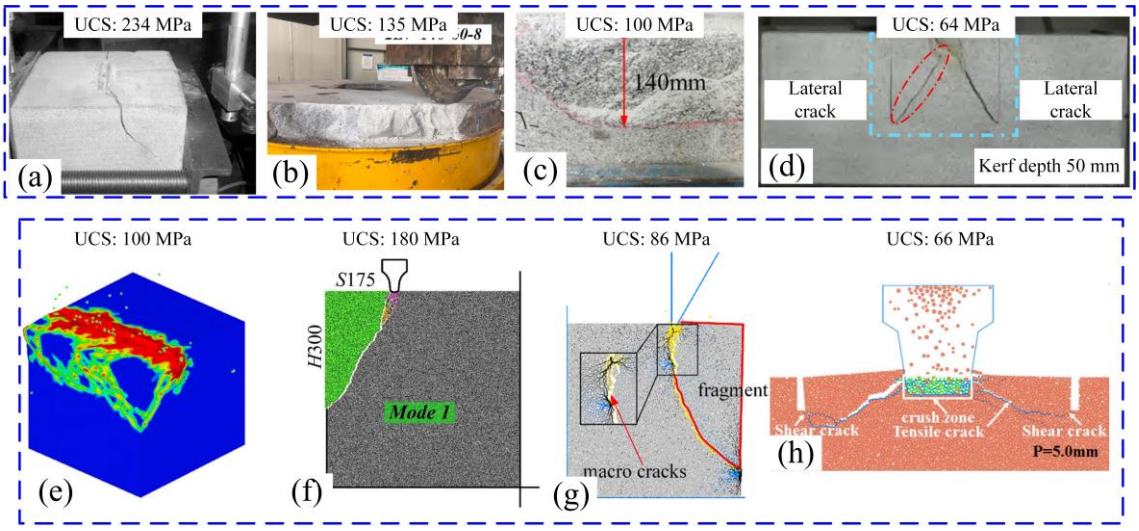

Fig. 13 - Representative studies of rock-breaking under different side-free-face conditions

***(a)** static penetration test on a diorite, D =75 mm, H =30 mm[10];**(b)** rotary cutting test on a granite, D =40~180 mm, H =140 mm[17];**(c)** linear cutting test on a granite, D =20~120 mm, H =200 mm[15]; **(d)** static penetration test on a sandstone, D =60 mm, H =0~50 mm[26]; **(e)** linear cutting simulation on a granite, D =20~120 mm, H =300 mm[15]; **(f)** static penetration simulation on a granite, D =75~200 mm, H =100~350 mm[14]; **(g)** static penetration simulation on a rock sample, D =5~30 mm, H =50 mm[12]; **(h)** static penetration simulation on a sandstone, D =30~45 mm, H =10 mm[23].*

CONCLUSION

In this study, to investigate the rock-breaking mechanism and then optimize the structure of the transition zone of the conical cutterhead, a rock-penetration numerical model is built using a grain-based discrete element method (GDEM) to synthesize rock. After the numerical model is verified, a group of simulations are conducted considering the influence of cutterhead conical angle, cutter spacing, and cutter tilt angle on the rock-breaking performance. The mainly analyzed indicators are the rock chipping, cutter penetration force, and penetration-specific energy. The rock-breaking mechanism of the cutters in the conical area of the conical-shaped cutterhead is free-face-assisted rock breaking. The rock-breaking force and efficiency of the tilt cutters are lower and higher than those of the normal cutters, respectively. Two key factors considering free face structure that affect rock-breaking performance are the free face height and the distance between the penetration point and the side free face. The two factors are then affected by cutter spacing and cutterhead conical angle. The rock-breaking efficiency increases with the increase of cutterhead conical angle but decreases with the increasing of cutter spacing and cutter tilt angle. For hard rock with a UCS of approximately 180 MPa, from the perspective of efficient rock breaking, it is preliminarily suggested that the tilt-cutters' spacing of the conical cutterhead should be less than 70 mm, cutterhead conical angle should be approximately 25°, and the cutter tilt angle should be no more than 3°. The conclusions drawn can provide a theoretical basis for the design of the conical TBM cutterhead.

CONFLICTS OF INTEREST

The authors declare no conflicts of interest.

DATA AVAILABILITY

All data, models, and code generated or used during the study appear in the submitted article.

ACKNOWLEDGMENTS

This work was supported by the Research Program of The Electricity Engineering CO.,LTD under CREC NO.5 Group (Grant number: 2022-DSZQ-007).

REFERENCES

[1] Rostami J., Chang S., 2017. A Closer Look at the Design of Cutterheads for Hard Rock Tunnel-Boring Machines. Engineering, Vol. 3, 892-904.
[2] Zhao Z.W., Zheng K.T., Li N., et al., 2016. Analysis on Static Mechanical Performances of TBM Cutterhead with Different Geometries. Tunnel Construction, Vol. 36, 102-107.
[3] Zhang Z.H., Li Z., Song C.N., 2018. Development and Challenge on Structural Design of Cutterhead of Full-face Rock TBM. Mining Machinery, Vol. 46, 1-7.
[4] Zhang Z.H., Chai C.Q., Zhao H., 2020. Research on Cutterhead Structural Design of TBM. Heavy Machinery, Vol. 13, 69-76.
[5] Zhang Z.H., 2003. Side Slip Analysis of Disc Cutter on Different Cutter Face of Roadheader. Modern Electric Power, Vol. 20, 16-18.
[6] Zhang Z.H., Sun F., 2016. Thrust Analysis of Full Face TBM with Conical Cutter Head during Operation. Construction Machinery, Vol. 47, 33-37.
[7] Zhang Z.H., Ji W., Weng Z.C., 2021. Determination Theory of Main Parameters and Simulation Analysis of the Conical Cutterhead Shield. Journal of Mechanical Engineering, Vol. 57, 243-255.
[8] Liu Y.Y., 2003. Determination of Type and Main Parameters of Full Face Rock Roadheader. Construction Machinery, Vol. 1, 11-15.
[9] Zhang H.X., Zhang N.C., 2007. Brief Discussion on Cutter Head Vibration of Type 803E TBM. Tunnel Construction, Vol. 12, 76-78.
[10] Innaurato N., Oggeri C., Oreste P.P., et al., 2007. Experimental and Numerical Studies on Rock Breaking with TBM Tools under High Stress Confinement. Rock Mechanics and Rock Engineering, Vol. 40, 429-451.
[11] Ramezanzadeh A., Hood M., 2010. A state-of-the-art review of mechanical rock exvacation technologies. International Journal of Medical Engineering and Informatics, Vol. 1, 29-39.
[12] Jiang H.X., Zhang X.D., Liu S.Y., et al., 2022. Research on the mechanism and performance of free-surface rock breakage by a disc cutter. Engineering Fracture Mechanics, Vol. 264, 108336.
[13] Geng Q., Wei Z.Y., Meng H., et al., 2016. Free-face-Assisted Rock Breaking Method Based on the Multi-stage Tunnel Boring Machine (TBM) Cutterhead. Rock Mechanics and Rock Engineering, Vol. 49, 4459-4472.
[14] Geng Q., Ye M., Lu Z.Y., et al., 2021. Numerical Study on Free Face-Assisted Rock Fragmentation Induced by a TBM Disk Cutter. 11th Conference of Asian Rock Mechanics Society.
[15] Xia Y. M., Guo B., Cong G. Q., et al., 2017. Numerical simulation of rock fragmentation induced by a single TBM disc cutter close to a side free surface. International Journal of Rock Mechanics and Mining Sciences, Vol. 91, 40-48.
[16] Zhang X.H., Xia Y.M., Zeng G., et al., 2018. Numerical and Experimental Investigation of Rock Breaking Method under Free Surface by TBM Disc Cutter. Journal of Central South University, Vol. 25, 2107-2118.
[17] Xu H.G., Geng Q., Sun Z.C., et al., 2021. Full-scale granite cutting experiments using tunnel boring machine disc cutters at different free-face conditions. Tunnelling and Underground Space Technology, Vol. 108, 103719.
[18] Wang K., 2020. Numerical Simulation Research on the Rock Fracturing by a TBM Disc Cutter Assisted by Free Faces. Journal of Railway Engineering Society. Vol. 37, 96-102.
[19] Shang X.N., Zhou J., Liu, F.S., et al., 2023. A peridynamics study for the free-surface-assisted rock fragmentation caused by TBM disc cutters. Computers and Geotechnics, Vol. 158, 105380.
[20] Bilgin, N., Copur, H., Balci, C., 2013. Mechanical excavation in mining and civil industries. CRC Press.
[21] Zhang J.L., Li Y., Zhang Y., et al., 2020. Using a high-pressure water jet-assisted tunnel boring machine to break rock. Advances in Mechanical Engineering, Vol. 12, 1-16.
[22] Geng Q., Lu Z.Y., Zhang Z.Y., et al., 2021. Numerical Simulation on the Rock Fragmentation Process Induced by Tunnel Boring Machine Disc Cutters Assisted by Pre-Cut Grooves. Journal of Xi'an Jiaotong University, Vol. 55, 9-19.

[23] Cheng J.L., Yang S.Q., Han W.F., et al., 2022. Experimental and numerical study on the indentation behavior of TBM disc cutter on hard-rock precutting kerfs by high-pressure abrasive water jet. Archives of Civil and Mechanical Engineering, Vol. 22, 1-23.
[24] Li B., Hu M.M., Zhang B., et al., 2022. Numerical simulation and experimental studies of rock-breaking methods for pre-grooving-assisted disc cutter. Bulletin of Engineering Geology and the Environment, Vol. 81, 90.
[25] Li B., Zhang B., Hu M.M., et al., 2022. Full-scale linear cutting tests to study the influence of pre-groove depth on rock-cutting performance by TBM disc cutter. Tunnelling and Underground Space Technology, Vol. 122, 104366.
[26] Zhou H., Xu F.T., Lu J.J., et al., 2022. Influence of pre-cutting groove on rock breaking mechanism of tunnel boring machine disc cutter. Rock and Soil Mechanics, Vol. 43, 625-634.
[27] Gong Q.M., Zhao J., Jiao Y.Y., 2005. Numerical modeling of the effects of joint orientation on rock fragmentation by TBM cutters. Tunnelling and Underground Space Technology, Vol. 20, 183-191.
[28] Li X.F., Li H.B., Liu Y.Q., et al., 2016. Numerical simulation of rock fragmentation mechanisms subject to wedge penetration for TBMs. Tunnelling and Underground Space Technology, Vol. 53, 96-108.
[29] Potyondy D.O., Cundall P.A., 2004. A bonded-particle model for rock. International Journal of Rock Mechanics and Mining Sciences, Vol. 41, 1329-1364.
[30] Ghazvinian E., Diederichs M.S., Quey, R., 2014. 3D random Voronoi grain-based models for simulation of brittle rock damage and fabric-guided micro-fracturing. Journal of Rock Mechanics and Geotechnical Engineering, Vol. 6, 506-521.
[31] Li X.F., Zhang Q.B., Li H.B., et al., 2018. Grain-Based Discrete Element Method (GB-DEM) Modelling of Multi-scale Fracturing in Rocks Under Dynamic Loading. Rock Mechanics and Rock Engineering, Vol. 51, 3785-3817.
[32] Li X.F., Li H.B., Zhao, J., 2017. 3D polycrystalline discrete element method (3PDEM) for simulation of crack initiation and propagation in granular rock. Computers and Geotechnics, Vol. 90, 96-112.
[33] Cho N., Martin C.D., Sego D.C., 2007. A clumped particle model for rock. International Journal of Rock Mechanics and Mining Sciences, Vol. 44, 997-1010.
[34] Balci C., Bilgin N., 2007. Correlative study of linear small and full-scale rock cutting tests to select mechanized excavation machines. International Journal of Rock Mechanics and Mining Sciences, Vol. 44, 468-476.
[35] Entacher M., Lorenz S., Galler R., 2014. Tunnel boring machine performance prediction with scaled rock cutting tests. International Journal of Rock Mechanics and Mining Sciences, Vol. 70, 450-459.
[36] Comakli R., Balci C., Copur H., et al., 2021. Experimental studies using a new portable linear rock cutting machine and verification for disc cutters. Tunnelling and Underground Space Technology, Vol. 108, 103702.
[37] Gong Q.M., Du X., Li, Z., et al., 2016. Development of a mechanical rock breakage experimental platform. Tunnelling and Underground Space Technology, Vol. 57, 129-136.
[38] Cho J.W., Jeon S., 2010. Optimum spacing of TBM disc cutters: A numerical simulation using the three-dimensional dynamic fracturing method. Tunnelling and Underground Space Technology, Vol. 25, 230-244.
[39] Pan Y.C., Liu, Q.S., Liu, J., et al., 2018. Full-scale linear cutting tests in Chongqing Sandstone to study the influence of confining stress on rock cutting efficiency by TBM disc cutter. Tunnelling and Underground Space Technology, Vol. 80, 197-210.
[40] Entacher M., Winter G., Bumberger T., et al., 2012. Cutter force measurement on tunnel boring machines-System design. Tunnelling and Underground Space Technology, Vol. 31, 97-106.